END

DATE
FILMED

1 - 77

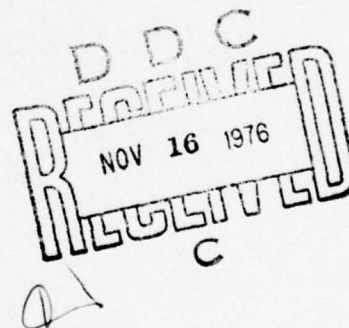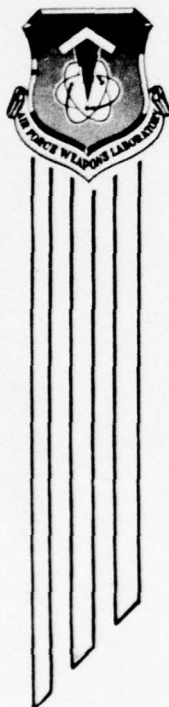AFWL-TR-76-128

AFWL-TR-
76-128

AD A032050

THE PERFORMANCE OF THE TATS WIDEBAND
MODEM IN SEVERELY SCINTILLATED ENVIRONMENTS

September 1976

Final Report

Approved for public release; distribution unlimited.

D D C
RECEIVED
NOV 16 1976
C

AIR FORCE WEAPONS LABORATORY
Air Force Systems Command
Kirtland Air Force Base, NM 87117

This final report was prepared by the Air Force Weapons Laboratory, Kirtland Air Force Base, New Mexico under Job Order 46950112. Capt Wittwer (DYT) was the Laboratory Project Officer-in-Charge.

When US Government drawings, specifications, or other data are used for any purpose other than a definitely related Government procurement operation, the Government thereby incurs no responsibility nor any obligation whatsoever, and the fact that the Government may have formulated, furnished, or in any way supplied the said drawings, specifications, or other data is not to be regarded by implication or otherwise as in any manner licensing the holder or any other person or corporation or conveying any rights or permission to manufacture, use, or sell any patented invention that may in any way be related thereto.

This report has been reviewed by the Information Office (OI) and is releasable to the National Technical Information Service (NTIS). At NTIS, it will be available to the general public, including foreign nations.

This technical report has been reviewed and is approved for publication.

LEON A. WITTWER
Captain, USAF
Project Officer   FOR THE COMMANDER

DONALD B. MITCHELL   JOHN S. DeWITT
Lt Colonel, USAF   Lt Colonel, USAF
Chief, Theoretical Branch   Chief, Technology Division

DO NOT RETURN THIS COPY. RETAIN OR DESTROY.

REPORT DOCUMENTATION PAGE		READ INSTRUCTIONS BEFORE COMPLETING FORM
1. REPORT NUMBER AFWL-TR-76-128	2. GOVT ACCESSION NO.	3. RECIPIENT'S CATALOG NUMBER
4. TITLE *(and Subtitle)* THE PERFORMANCE OF THE TATS WIDEBAND MODEM IN SEVERELY SCINTILLATED ENVIRONMENTS.		5. TYPE OF REPORT & PERIOD COVERED Final Report. 6. PERFORMING ORG. REPORT NUMBER
7. AUTHOR(s) Leon A. Wittwer, Captain, USAF Erle Pettus, Lieutenant, USAF		8. CONTRACT OR GRANT NUMBER(s)
9. PERFORMING ORGANIZATION NAME AND ADDRESS Air Force Weapons Laboratory (DYT) Kirtland AFB, NM 87117		10. PROGRAM ELEMENT, PROJECT, TASK AREA & WORK UNIT NUMBERS JON 46950112 64711F
11. CONTROLLING OFFICE NAME AND ADDRESS Air Force Weapons Laboratory Kirtland AFB, NM 87117		12. REPORT DATE September 1976 13. NUMBER OF PAGES 44
14. MONITORING AGENCY NAME & ADDRESS*(if different from Controlling Office)*		15. SECURITY CLASS. *(of this report)* Unclassified 15a. DECLASSIFICATION/DOWNGRADING SCHEDULE

16. DISTRIBUTION STATEMENT *(of this Report)*

Approved for public release; distribution unlimited.

17. DISTRIBUTION STATEMENT *(of the abstract entered in Block 20, if different from Report)*

18. SUPPLEMENTARY NOTES

19. KEY WORDS *(Continue on reverse side if necessary and identify by block number)*

Scintillations
Ionospheric Propagation
Radio Propagation
UHF Propagation
Striations

20. ABSTRACT *(Continue on reverse side if necessary and identify by block number)*

The performance of the Tactical Transmission System (TATS) wideband modem is examined in scintillated environments. The analysis included both acquisition of signal and decoding behavior. The effects of time and frequency tracking errors were also included.

DD FORM 1473 1 JAN 73   EDITION OF 1 NOV 65 IS OBSOLETE

013150

CONTENTS

ILLUSTRATIONS

SECTION I

INTRODUCTION

The primary purpose of this report is twofold. First it demonstrates the performance to be expected of the Tactical Transmission System (TATS) wideband modem in scintillated environments in both nuclear and ambient environments. Second, this study demonstrates some of the basic characteristics of UHF scintillated signal structures as they are presently understood.

This report consists of five sections, which discuss, in turn, the environment and propagation, the TATS system, the hardware model, the simulation results, and the conclusions.

SECTION II

ENVIRONMENT AND PROPAGATION

The propagation environment geometry assumed here is representative of a link from equatorial synchronous orbit to midlatitude. The environment is defined by the ionospheric mean electron density, $\bar{n}$, the relative mean square electron density fluctuation power, $\overline{(n-\bar{n})^2}/\bar{n}^2$, and the correlation function of the electron density fluctuations. Figure 1 contains the mean electron density profile used in this study as a function of both the altitude and the line of sight (LOS) distance from the ground. The relative fluctuation power is varied to simulate varying degrees of scintillation effects. The electron density fluctuation correlation function is

$$R(r,z) = \overline{(n-\bar{n})^2} \left[\frac{e^{-c/L} e^{-(r^2+a^2z^2)^{1/2}/L} - e^{-c/\ell} e^{-(r^2+a^2z^2)^{1/2}/\ell}}{\left[e^{-c/L} - e^{-c/\ell} \right]} \right] \qquad (1)$$

where

$c = \ell L \ln (\ell/L)/(\ell-L)$

ℓ = inner scale size perpendicular to LOS

L = outer scale size perpendicular to LOS

$a = L/L'$

L' = outer scale size parallel to LOS

z = coordinate along the propagation LOS

r = cylindrically symmetric coordinate perpendicular to LOS

$\overline{(n-\bar{n})^2}$ = mean square electron density fluctuation

This function has the desirable properties of having an inner scale size, an outer scale size, and a zero slope at $r=z=0$. This correlation function corresponds to a K^{-2} spectrum for sizes smaller than L but larger than ℓ and K^{-4} for sizes smaller than ℓ. This spectrum is characteristic of most electron density measurements to date (refs. 1 and 2). Sagalyn (ref. 1) reports that this spectrum is typical of over 90 percent of the spectra analyzed at AFGL.
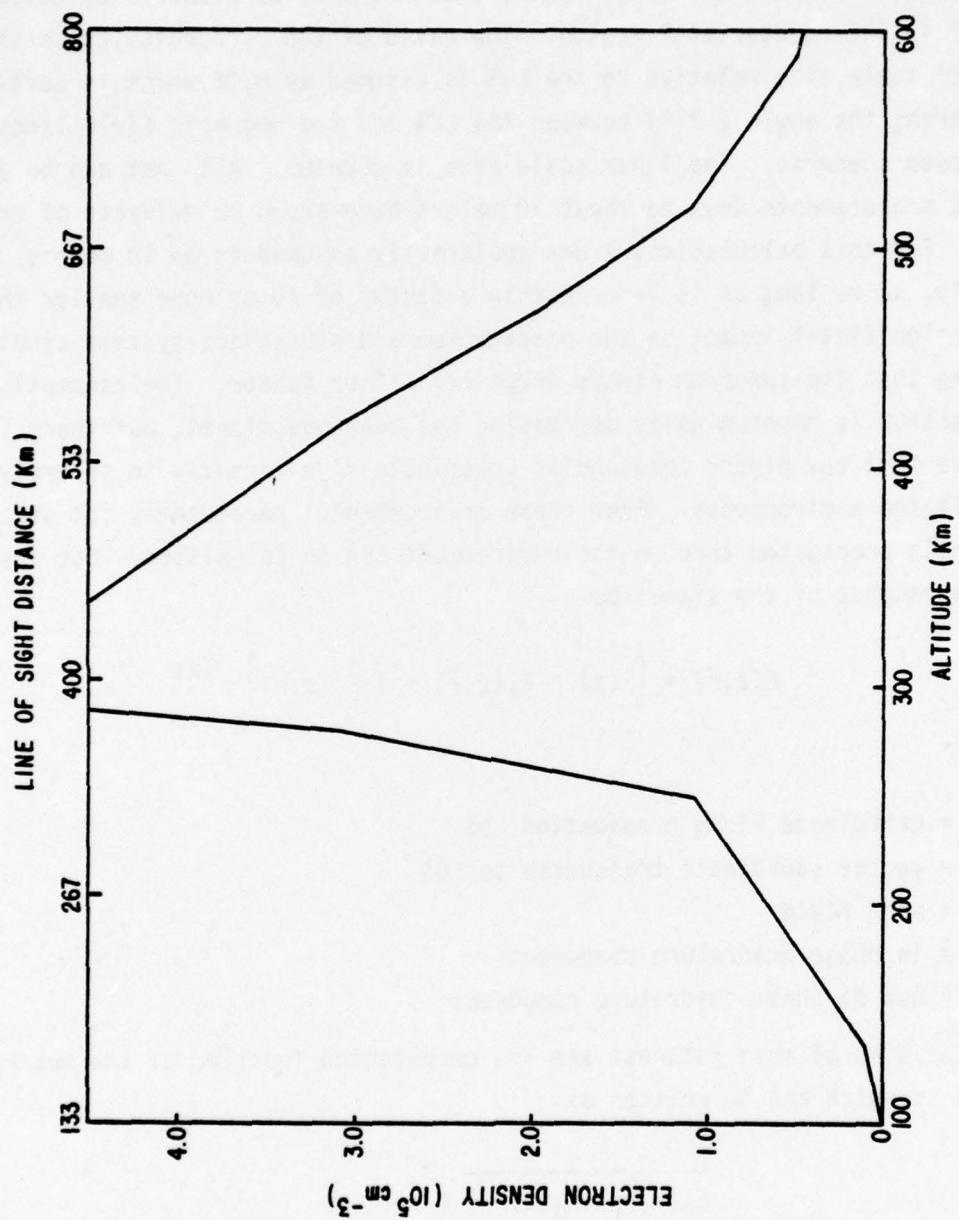
4

Figure 1. Model Ionosphere

This spectrum has also been calculated at NRL* in one of the most detailed calculations to date.

The outer scale size, L, is set at 1.25 km, a value measured by Kelley and Mozer** in the equatorial F region. The ratio of the perpendicular to the parallel scale size relative to the LOS is assumed as 0.36 which is derived by considering the angle (~21°) between the LOS and the magnetic field lines in the chosen scenario. The inner scale size is unknown. All that can be said is that measurements down to about 30 meters have shown no evidence of an inner scale. For this calculation, ℓ was arbitrarily assumed to be 10 meters. Fortunately, ℓ, as long as it is more than a factor of 10 or more smaller than L, has no significant impact on the propagation and subsequent systems studies assuming that the spectrum always drops off K^{-2} or faster. The assumption that the spectrum is monotonically decreasing has been questioned, but there is no evidence that the higher frequencies contribute significantly in severely scintillated environments. From these environmental parameters, the statistics of signals propagated through the environment can be calculated. Let the spatial dependence of the signal be

$$E(z,\overline{r}) = \left[\overline{E}(z) + E_R(z,\overline{r}) + i\, E_I(z,\overline{r})\right] e^{iKz} \tag{2}$$

where

z = coordinate along propagation LOS

$\overline{r}$ = vector coordinate transverse to LOS

$\overline{E}$ = mean field

E_R = in phase quadrature component

E_I = out of phase quadrature component

The quantities of most interest are the correlation function of the quadrature components which can be written as

$$\overline{E_R(z,\overline{r}_1)\, E_R(z,\overline{r}_2)} = H_R(z,r) \tag{3a}$$

---

* Scannapieco, A.J., Ossakow, S.L., Goldman, S.R., and Pierre, J.M., "Late-Time Striation Spectra," Naval Research Laboratory, Private Communication, February 1976.

**Kelley and Mozer, Private Communication.

$$\overline{E_I(z,\overline{r}_1) \, E_I(z,\overline{r}_2)} = H_I(z,r) \tag{3b}$$

$$\overline{E_R(z,\overline{r}_1) \, E_I(z,\overline{r}_2)} = H_{RI}(z,r) \tag{3c}$$

where $r = |\overline{r}_1 - \overline{r}_2|$ since the correlation function of the electron density fluctuations is cylindrically symmetric.

The F and G functions are then defined

$$G(z,r) = \overline{E(z)}^2 + H_R(z,r) + H_I(z,r) \tag{4a}$$

$$H(z,r) = \overline{E(z)}^2 + H_R(z,r) - H_I(z,r) + 2i \, H_{RI}(z,r) \tag{4b}$$

The calculation of the F and G functions from the electron density correlation function has been described elsewhere (ref. 3) and will not be discussed here. The decorrelation distance (r_o) of the signal structure is defined to be the 1/e point of $G(z,r) - \overline{E(z)}^2$ where z is the receiver coordinate. An important limit occurs when $\overline{E(z)}$ gets small. Then

$$H_R(z,r) = H_I(z,r) \tag{5a}$$

$$H_{RI}(z,r) = 0 \tag{5b}$$

Since we will assume that $E_R(z,\overline{r})$ and $E_I(z,\overline{r})$ are zero mean gaussian variables, the above limit is equivalent to Rayleigh statistics. Given $G(z,r)$, $F(z,r)$, $\overline{E(z)}$, and the gaussian assumption on the quadrature components, we have a complete statistical description of the spatial signal structure.

To convert spatial statistics to time statistics, assume that the characteristic velocity of the LOS relative to the electron density fluctuations is $\overline{v} = 400$ meters/second. This velocity is a reasonable upper limit for ambient environments but may be somewhat low for certain nuclear environments. The space-velocity transformation is

$$\tau = \frac{r}{\overline{v}} \tag{6}$$

Procedures for generating signal samples from the time statistics are described in the appendix.

Five propagation calculations were run varying the relative fluctuation power, $\overline{(n-\overline{n})^2}/\overline{n}^2$. Table 1 summarizes the calculated environments along with three extrapolated environments.

Table 1

PROPAGATION CALCULATIONS

$\overline{(n-\overline{n})^2}/\overline{n}^2$	$E(z)^2$	$\tau_0(\text{sec})$	$\int \overline{(n-\overline{n})^2}dz$
10^{-4}	0.74	2.6	4.21×10^{14}
10^{-3}	0.05	1.9	4.21×10^{15}
10^{-2}	4.1×10^{-14}	0.4	4.21×10^{16}
10^{-1}	1.34×10^{-134}	0.1	4.21×10^{17}
10^{0}	~ 0	2.6×10^{-2}	4.21×10^{18}
3.07	~ 0	1.3×10^{-2}	1.29×10^{19}
9.45	~ 0	6.5×10^{-3}	3.98×10^{19}
29.04	~ 0	3.2×10^{-3}	1.22×10^{20}

where $\tau_0 = r_0/\overline{v}$ is the decorrelation time of the signal structure. The last three entries are cases extrapolated from the $\tau_0 = 0.026$ case. To perform the extrapolation, $\int (n-\overline{n})^2$ dz corresponding to the new assumed values of τ_0 must be obtained. The extrapolated values can be found for $\int \overline{(n-\overline{n})^2}dz$ by looking at figure 2 which relates the pertinent quantities. The results in this figure are from a large number of calculations varying the various environmental parameters. For scattering layers where the environmental parameters are constant, figure 2 can be simply summarized.

$$\tau_0 = \text{minimum} \left[1.3L, \frac{\dfrac{2.4 \times 10^{14} \, L \, K^{1.23}}{\left(\overline{(n-\widetilde{n})^2} \, z \, L'\right)^{0.616}}}{\overline{v}} \right] \qquad (6)$$

where z is the layer thickness and K is the signal wave number.

This extrapolation to different environments is valid since the correlation functions of the quadrature signal components of the $\tau_0 = 0.026$ second case are near gaussian in shape. The gaussian shape is the limiting form as the
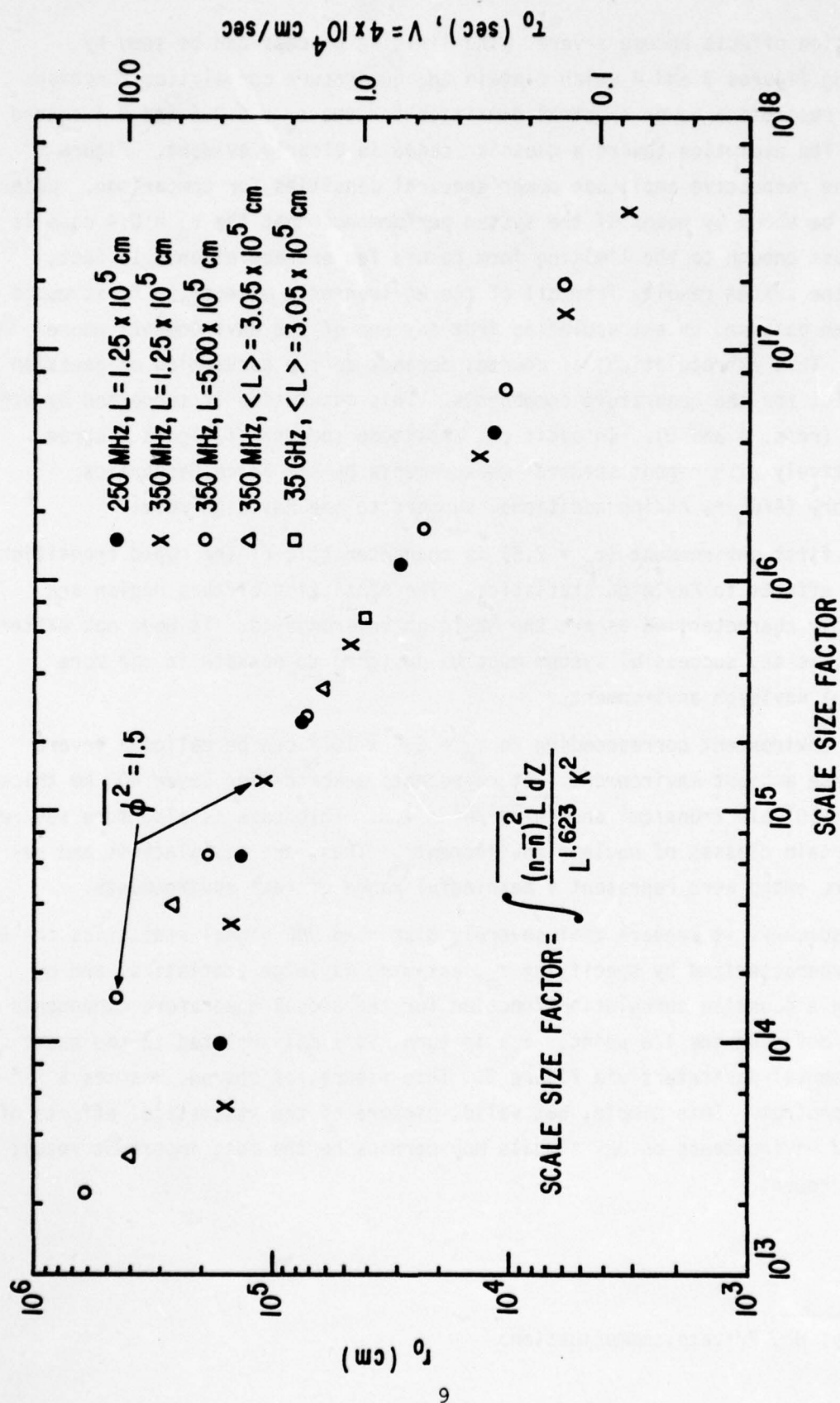
8

Figure 2. Decorrelation Distance (r_o) Versus Scale Size Factor

$$\text{SCALE SIZE FACTOR} = \int \frac{\sqrt{\overline{(n-\bar{n})^2}}\, L'\, dZ}{L^{1.623}\, K^2}$$

propagation effects become severe. The limiting process can be seen by examining figures 3 and 4 which contain the quadrature correlation functions and the respective power spectral densities for the τ_0 = 0.026 and 0.4 second cases. The evolution toward a gaussian shape is clearly evident. Figure 5 shows the respective amplitude power spectral densities for comparison. Later, it will be shown by means of the system performance that the τ_0 = 0.4 case is also close enough to the limiting form to use for extrapolation. In fact, all of the system results from all of the environments except the first could have been obtained by extrapolation from any one of the environments where $\tau_0 \leq 2$. This extrapolation, of course, depends on the assumption of gaussian statistics for the quadrature components. This assumption is supported by other studies (refs. 4 and 5). In addition, amplitude spectra of figure 5 agree qualitatively with recent spectral measurements by Air Force Geophysics Laboratory (AFGL)*, adding additional support to the Rayleigh model.

The first environment (τ_0 = 2.6) is characteristic of the rapid transition from no effects to Rayleigh statistics. The statistics of this region are not simply characterized as are the Rayleigh environments. It does not matter, however, as any successful system must be designed to operate in the more stressful Rayleigh environments.

The environment corresponding to τ_0 = 6.5 x 10^{-3} can be called a severe worst case ambient environment. It represents a scattering layer 400 km thick with $\bar{n}$ = 10^6 electrons/cm³ and $\overline{(n-\bar{n})^2}/\bar{n}^2$ = 1.0. This case is also more severe than certain classes of nuclear environments. Thus, the calculations and results presented here represent a meaningful range of real environments.

In summary, it appears that severely disturbed UHF signal statistics can be simply characterized by specifying τ_0, assuming Rayleigh statistics, and by assuming a gaussian correlation function for the signal quadrature components with τ_0 defining the 1/e point. τ_0, in turn, is simply related to the basic environmental parameters via figure 2. This figure, of course, assumes a K^{-2} power spectrum. This simple, but valid, picture of the statistical effects of striated environments on UHF signals may perhaps be the most important result in this report.

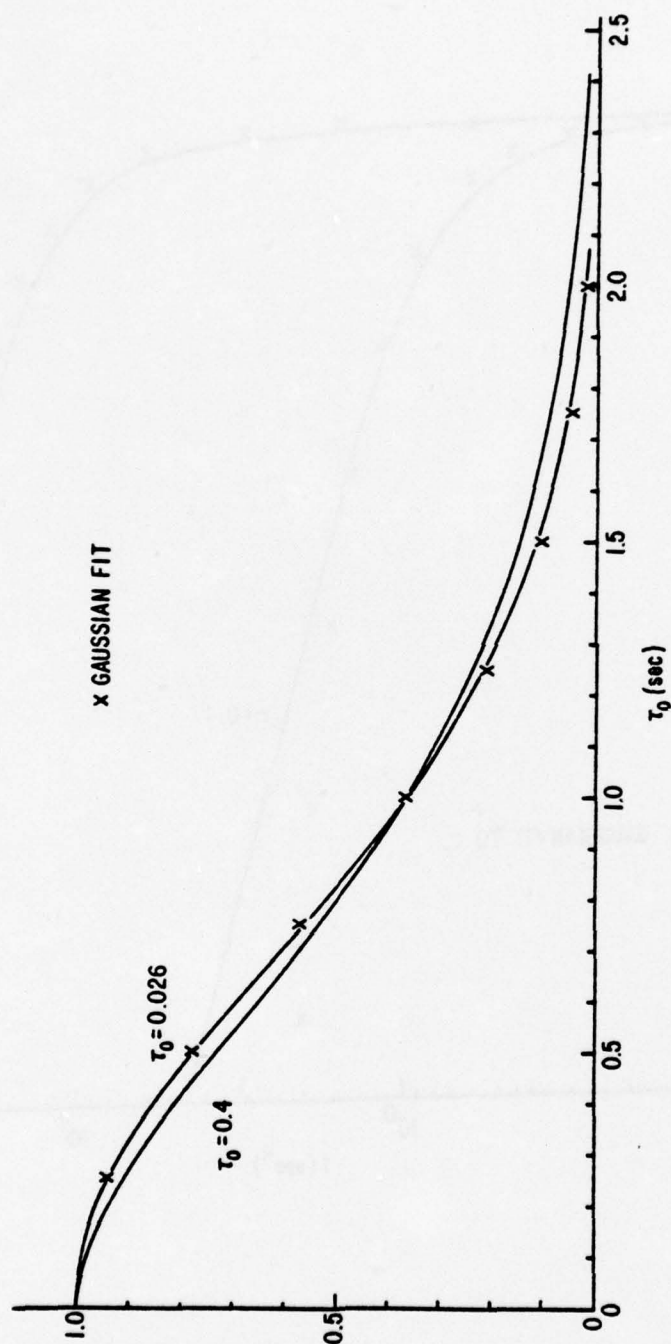*Whitney, H., Private communication.

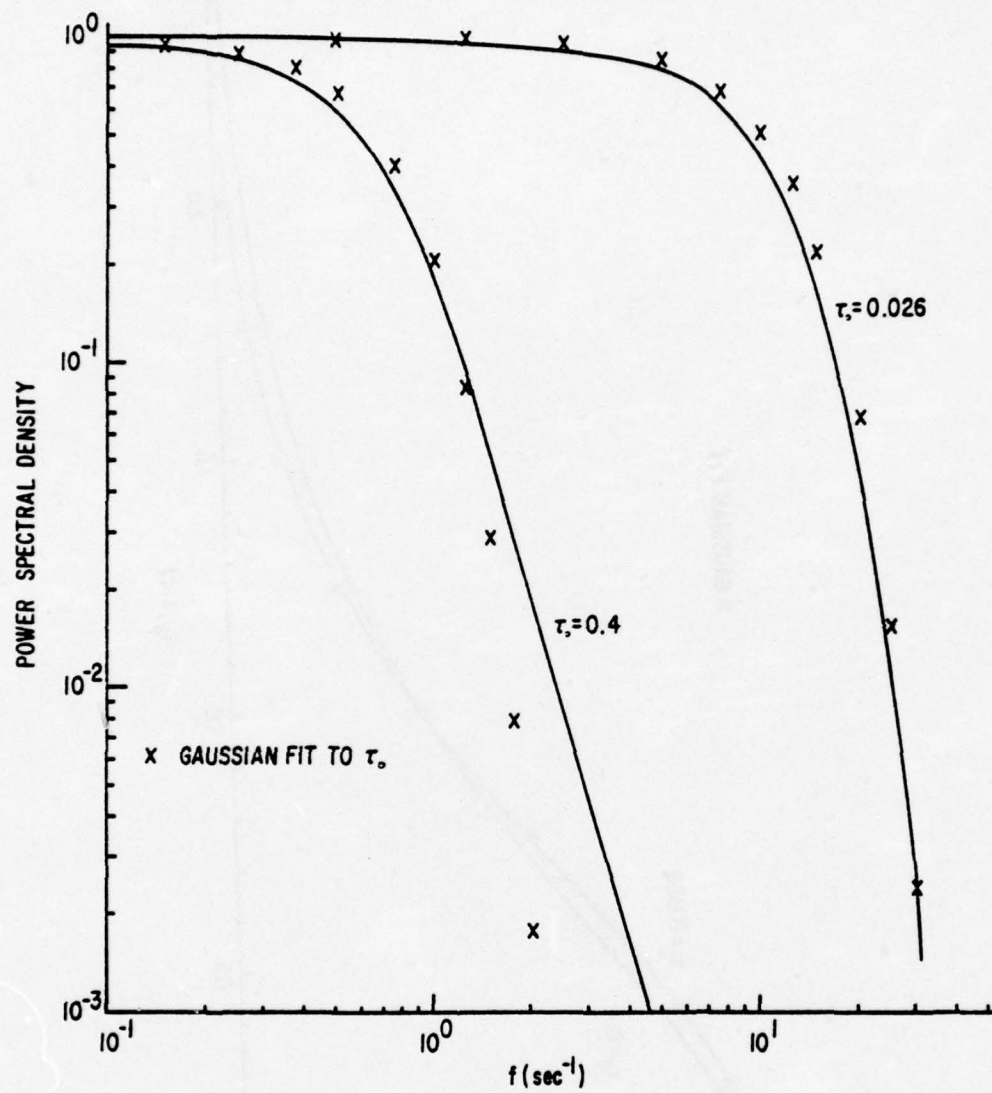Figure 3. Quadrature Component Correlation Functions

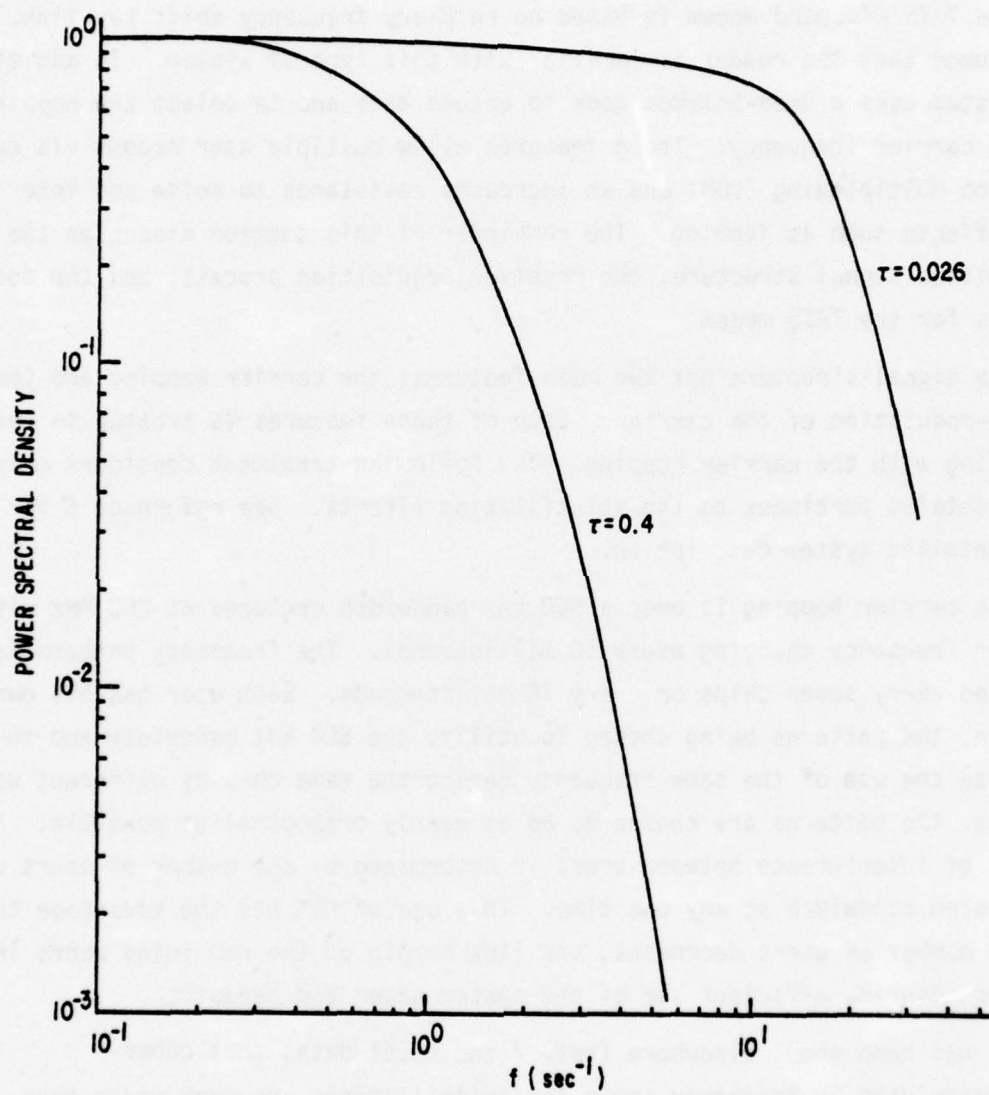Figure 4. Quadrature Component Power Spectral Density

Figure 5. Amplitude Power Spectral Density

SECTION III

TATS WIDEBAND SYSTEM DESCRIPTION

The TATS wideband modem is based on an 8-ary frequency shift key link. It is assumed that the reader is familiar with this type of system. In addition, the system uses a Reed-Solomon code to encode data and to select the hopping of the carrier frequency. These features allow multiple user access via code division multiplexing (CDM) and an increased resistance to noise and interference effects such as jamming. The remainder of this section discusses the transmitted signal structure, the receiver acquisition process, and the decoding process for the TATS modem.

The signal structure has two main features; the carrier hopping and the coding-modulation of the carrier. Each of these features is treated in turn beginning with the carrier hopping. The following treatment considers only those details pertinent to the scintillation effects. See reference 6 for a more detailed system description.

The carrier hopping is over a 500 kHz bandwidth centered at 260 MHz with the carrier frequency changing every 10 milliseconds. The frequency pattern is repeated every seven chips or every 70 milliseconds. Each user has his own pattern, the patterns being chosen to utilize the 500 kHz bandwidth and to minimize the use of the same frequency during the same chip by different users; that is, the patterns are chosen to be as nearly orthogonal as possible. The amount of interference between users is determined by the number of users using the system bandwidth at any one time. This use of CDM has the advantage that as the number of users decreases, the link margin of the remaining users increases insuring efficient use of the system power and bandwidth.

It has been shown elsewhere (ref. 7 and NELC* data) that coherence bandwidths in frequency space for scintillations are much wider than 500 kHz so it is reasonable to ignore frequency selectivity over the hopping bandwidth. The degradation of the signals due to the presence of other users is also ignored in this study. These two assumptions mean that the details of

---

*Private communication.

the carrier frequency hopping need not be explicitly modeled. The details of
the information coding, however, must be modeled in detail.

The information coming into the modulator is in terms of 6 bit characters.
These characters are encoded using a Reed-Solomon code where each of the 6 bit
characters is represented by a sequence of seven numbers, each number ranging
from 0 to 7. The sequences for each character are chosen to minimize the
occurrence of the same number in the same position in the 7 number sequence
for any two characters, that is, maximize character orthogonality. For the
code used here, a particular character representation has no numbers in its
sequence in common with 14 other characters and only one number in common with
the remaining 49 characters. The use of these nearly orthogonal representations
results in a significant improvement in performance over noncoded schemes.

A coded character is modulated onto the carrier frequency in a sequence
of eight chips, the last seven chips corresponding to the sequence of seven
numbers of the Reed-Solomon character representation. The first chip is at
the carrier frequency and is used to track time and frequency changes. Each
chip is modulated using an 8-ary frequency shift key (FSK) modulation. In
this modulation, each of the eight possible number values in the Reed-Solomon
code is represented by a discrete frequency relative to the carrier frequency.
For example, the 6 bit character 100101 is represented by the sequence
(1,2,3,7,5,0,6). The code word representation in frequency space is shown
in figure 6. "f_c" is the carrier frequency and Δf = 100 Hz.

It is important to note that a code word is one chip longer than the
carrier frequency hopping pattern. As a result, the synchronization chip at
the carrier frequency is rotated through the carrier hopping pattern giving
a measure of frequency diversity protection to the synchronization process.

The signal structure development for information transmission can be
summarized as follows. During transmission, a 6 bit information character is
put into the coder, which converts it, using a Reed-Solomon code, to a sequence
of seven numbers ranging from 0 to 7. The Reed-Solomon sequence is modulated
on seven chips of the carrier frequency using an 8-ary FSK modulation. An
unmodulated synchronization chip precedes each 7 chip sequence and the 8 chips
together represent the original 6 bit information character. Finally, the
carrier frequency is hopped over a 500 kHz bandwidth every chip. During
acquisition, the signal structure is somewhat different. First there are 532
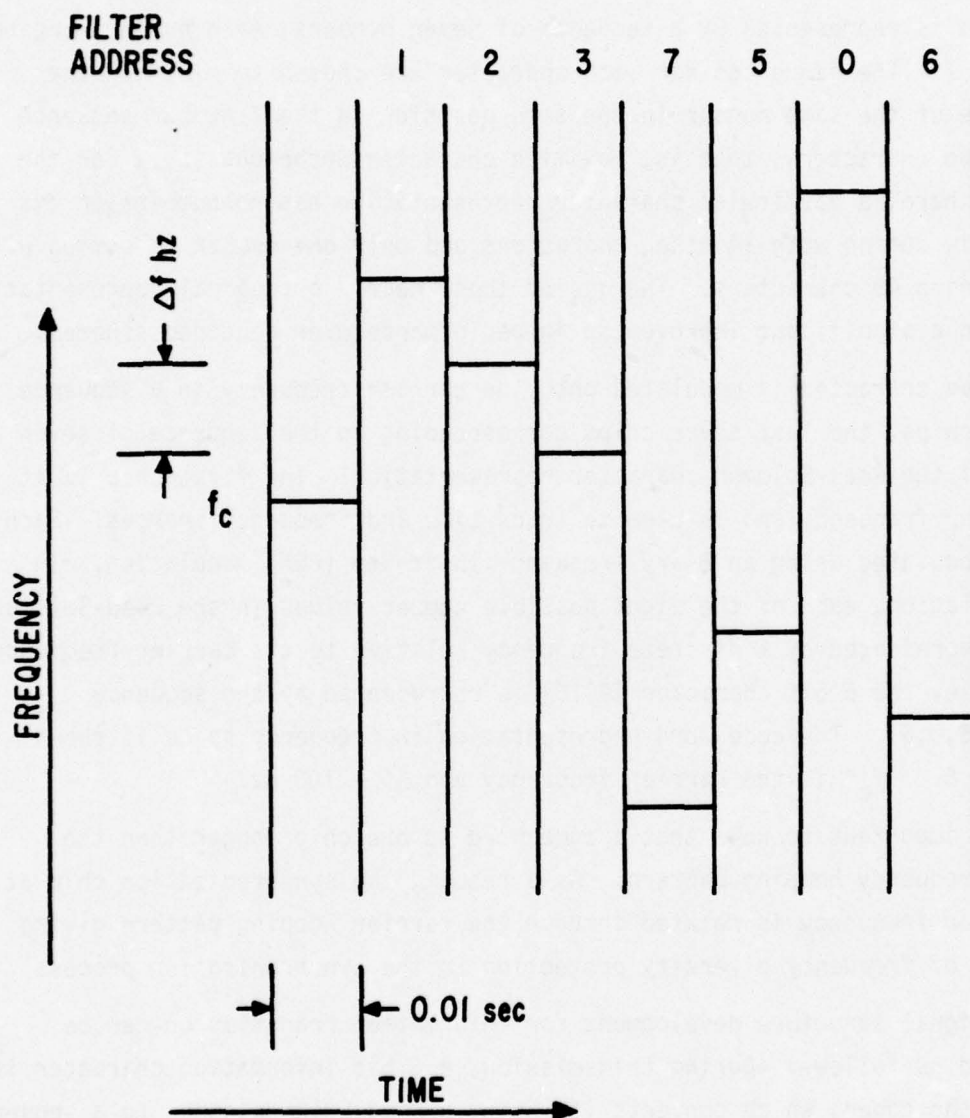chips of unmodulated hopped carrier. Since each user has his own pattern, this

15

Figure 6. (1,2,3,7,5,0,6) Reed-Solomon Character

chip sequence acts as a user address. The user employs the sequence to acquire and pull in both time and frequency synchronization. Four start-of-message characters follow this chip sequence. These characters have the same structure as information characters except no synchronization chips are used. These characters are also sent having each 7 chip sequence in time with the 7 chip carrier frequency hopping pattern.

Next, it is necessary to know the procedure used by the demodulator to recognize the signal. The hopping pattern recognition process is carried out by eight matched filters that are also used to decode the information characters. The filters are separated by 100 Hz; thus, the frequency uncertainty that can be initially handled is about ±400 Hz. (In practice, this range can be increased by shifting the initial carrier frequency estimate to widen the coverage of the eight matched filters in frequency space.) When searching for its pattern, the receiver dehops the carrier and feeds the result to eight matched filters each of which is followed by an envelope detector. The quantized outputs of each filter-envelope detector are sampled at $T/2$ and T relative to the receiver. The outputs are accumulated in 16 accumulators, 2 for each filter. If, at the end of 21 chips, none of the 16 accumulators has exceeded a preset threshold of 110, the accumulators are cleared, the dehopping pattern is slipped a chip in timing, and another 21 chip search is done. This process continues until the local dehopping pattern is within about $T/2$ seconds time synchronization with the sender hopping pattern. When this occurs, given sufficient power and given that the carrier frequency is not in error by more than about ±400 Hz, one of the 16 accumulators should exceed the preset threshold because at least one of the filters must be close to the frequency being sent and the filter integration ending at $T/2$ or T must overlap the signal sent. When an accumulator exceeds the threshold, the accumulator address is stored, the accumulators are cleared, and another 21 chip search is initiated but without changing the dehopping timing. If the same accumulator again exceeds the threshold within 21 chips, the receiver assumes its pattern is being sent. The 532 chips allow for two chances to recognize the pattern before a failure will occur. If the pattern recognition occurs near the end of the 532 chips, sufficient chips may not remain to finish the acquisition process.

Once the pattern has been recognized, the receiver does an initial time and frequency correction based on the address of the accumulator that exceeded the threshold. If the accumulator corresponded to a sample at T, the timing

17

is retarded by $T/4$; otherwise no correction is made. The frequency shift of the filter where the signal was found is added to the initial carrier frequency estimate correcting that quantity. With these initial corrections, the receiver proceeds to pull in the time and frequency track more accurately.

The time and frequency tracking are done with three matched filters. For frequency tracking two filters, tuned to $f_c \pm \Delta f/2$ where f_c is the carrier frequency estimate resulting from the hopping pattern recognition process, are used. These filters integrate over the chip period and the quantized outputs are compared. If the $f_c + \Delta f/2$ output is greater, a counter is increased by one. If the $f_c - \Delta f/2$ output is greater, the counter is decreased by one. If the counter value becomes greater than NC, the counter is zeroed and f_c is increased by $\Delta f/8$. If the counter value is less than -NC, f_c is corrected the other way. Thus, the carrier frequency estimate is continually adjusted toward the real carrier frequency. The timing is handled much the same way. A filter tuned to the carrier frequency estimate is sampled at $T/2$ and T and the quantized outputs are compared. If the T output is greater, another counter is increased by one. If the $T/2$ output is greater, the counter is decreased. The timing is corrected by $\pm T/32$ whenever the timing counter exceeds NC or is less than -NC, respectively. In this tracking mode, the system tracks for 98 chips with NC = 3 and then for another 98 chips with NC = 7. After the 196 chips have been processed, the timing and frequency are presumably sufficiently accurate to look for the start of message characters.

The system looks for the start of message characters for 343 chips and goes back to the hopping pattern search if they are not found. The search for the 4 characters is done by the same procedure as the decoding of the information characters with two differences. First, there are no synchronization chips. Second, the criterion for acceptance includes the sum of the 4 start-of-message character accumulators being greater than 245 as well as recognition of the individual characters. After these characters are found, the system has time, frequency, and character synchronization, and information decoding can begin.

When information is being received, the receiver is carrying out three basic functions. First, it maintains time and frequency synchronization using the synchronization chip at the beginning of each character. The procedure for this chip is identical to that used in the initial pull-in during acquisition

18

with NC = 7. The maximum tracking rates are easy to estimate. The timing loop
can track up to about 5×10^{-4} sec/sec. The frequency loop can track up to about
19.5 Hz/sec.

The second and most important function is to decode the Reed-Solomon code.
To each of the 64 characters, there corresponds an accumulator represented
schematically in figure 7. As each chip is processed through the matched
filter bank, each character accumulator receives the quantized output from the
appropriate filter. For example, the 100101 character discussed earlier is
the 38th character; thus, the 38th accumulator receives successively quantized
outputs from filters 1,2,3,7,5,0, and 6. At the end of the seven chips, all
of the accumulators are compared and the character corresponding to the accumu-
lator with the largest value is inputted into the data stream. For the present
work, random characters were used and the results are in terms of 6 bit charac-
ter error rates.

The final function performed during information decoding is detecting
loss of message. This is accomplished by sampling the largest value from
the character accumulators at the end of each character. If three out of
four successive values, where one of the three must be the first, is below
a threshold of 70, the system starts a time-out counter. If four successive
character values that exceed the threshold are not found within 6 seconds,
the system stops decoding and returns to a pattern hopping search mode. If
the four character values are found, the system returns to its normal decoding
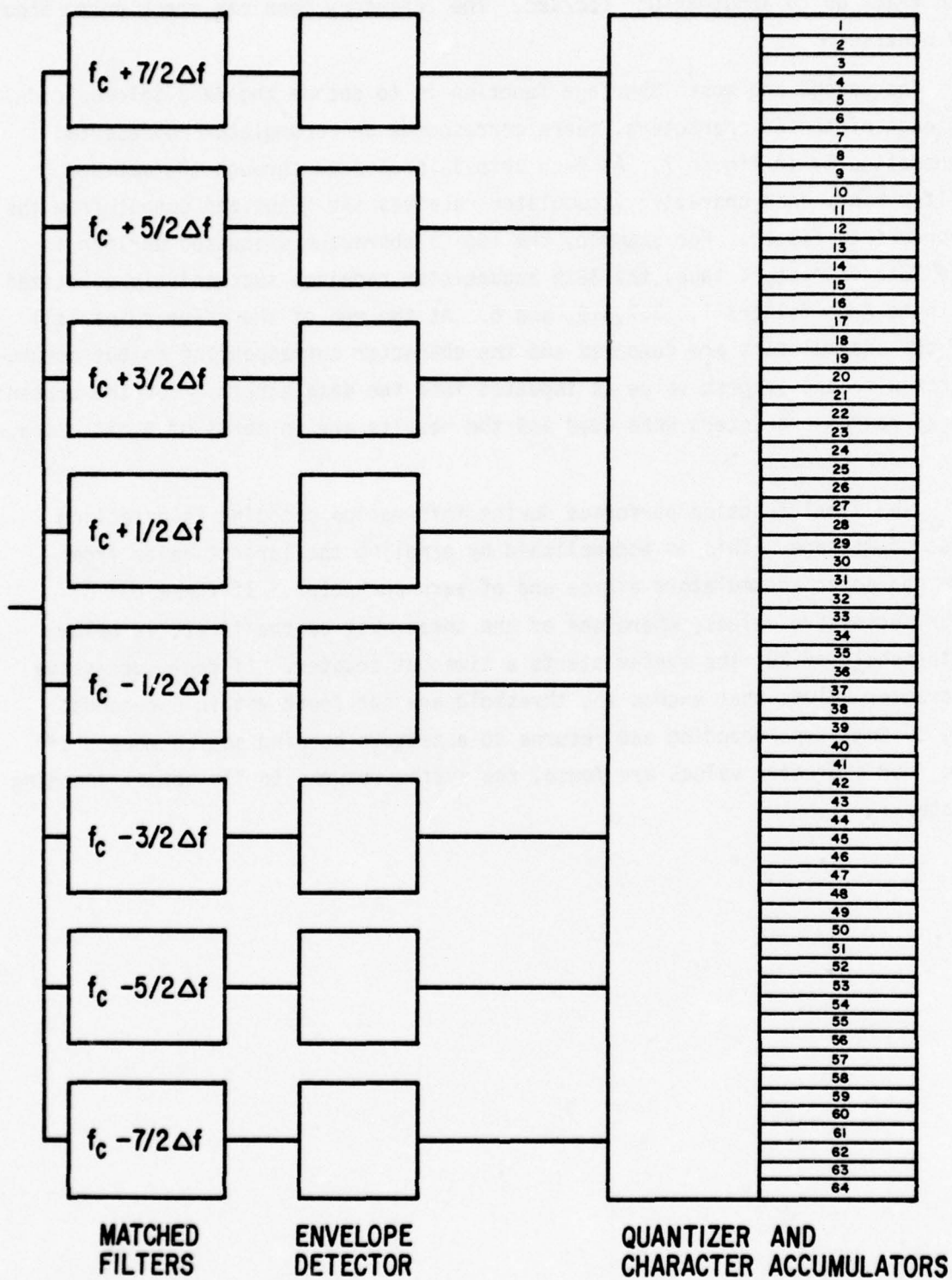state.

Figure 7. 8-ary Demodulator

20

SECTION IV

HARDWARE MODEL

As shown in the previous section, the acquisition, decoding, and other system functions are based on comparisons of the quantized outputs of the matched filter-envelope detector hardware. To calculate these outputs it was necessary to develop computer algorithms simulating the system hardware including the automatic gain control (AGC). This section considers the model formalism used to provide an accurate, efficient simulation of the hardware functions. First, the matched filter model is described as follows.

The received signal is represented as

$$S(t) = E(t)e^{i2\pi(f_c + \ell\Delta f/2)t} + n(t) \tag{7}$$

where

$E(t) = \overline{E} + E_R(t) + i\,E_I(t)$

f_c = carrier frequency

$\ell = \pm1, \pm3, \pm5, \pm7$ = frequency shift index

Δf = filter frequency separation

$n(t)$ = white gaussian noise input

$E(t)$ is the same as $E(\overline{r},z)e^{-iKz}$ in equation 2 with $t = |\overline{r}|/\overline{v}$ and z equal to the receiver coordinate. The output of the matched filter corresponding to the mth frequency shift with the ℓth shift present is

$$R_{m\ell} = \frac{E_o}{N} \int_{t'}^{t'+T'} E(t)e^{i2\pi[(\ell-m)\Delta f/2 + f_e]t} \, dt$$

$$+ \frac{E_o}{N} \int_{t'}^{t'+T'} n(t)e^{-i2\pi(m\Delta f/2 + f_c')t} \, dt \tag{8}$$

where

N = unilateral power spectral noise density

E_o = undisturbed field level

f_c' = demodulator carrier frequency estimate

$f_e = f_c - f_c'$

$T' = T - |T_e|$

T = chip period

T_e = timing error

The filter output in equation 9 is divided into three contributions. The first two result from dividing the first integral into low and high frequency signal portions and the last is noise. The low frequency portion of $E(t)$ is generated using Fourier techniques described in the appendix and is represented as a Fourier series.

$$E_{LF}(t) = \frac{1}{2L} \sum_{n=-n_c}^{n_c} C_n e^{i\frac{n\pi t}{L}} \tag{9}$$

where $n_c = L/T$; $2L$ is the time domain of the Fourier expansion and is chosen much larger than the correlation time, τ_o, of the signal structure. The resolution of $E_{LF}(t)$, Δt, is chosen to be greater than or equal to T. During each Δt, $E_{LF}(t)$ is assumed linear. Let

$$a = \frac{(E_{LF}(t+\Delta t) - E_{LF}(t))}{\Delta t} \tag{10a}$$

$$b = E_{LF}(t) \tag{10b}$$

The contribution to $R_{m\ell}$ from $E_{LF}(t)$ can be written as

$$R_{m\ell}\bigg|_{LF} = \frac{E_o}{N} \int_{t'}^{t'+T'} (at + b) \, e^{i2\pi[(\ell-m)\Delta f/2 + f_e]t} \, dt \tag{11}$$

22

•

where the range of the integral is in the Δt interval fit by a and b. After a change of variables,

$$R_{m\ell}\bigg|_{LF} = \frac{E_o}{N} e^{i2\pi[(\ell-m)\Delta f/2 + f_e]} \int_0^{T'} [a\tau + (b + at')] e^{i2\pi[(\ell-m)\Delta f/2 + f_e]\tau} dt \quad (12)$$

Finally,

$$R_{m\ell}\bigg|_{LF} = e^{i2\pi[(\ell-m)\Delta f/2 + f_e]t'} \left[a\, H_{m\ell}(T', f_e) + b'\, G_{m\ell}(T', f_e) \right] \quad (13)$$

where

$$G_{m\ell}(T', f_e) = \frac{iE_o}{\pi\Delta f(m-\ell)N} \left(e^{i2\pi[(\ell-m)\Delta f/2 + f_e]T'} - 1 \right) \quad (14)$$

$$H_{m\ell}(T', f_e) = \frac{iE_o}{\pi\Delta f(m-\ell)N} \left[T' e^{i2\pi[(\ell-m)\Delta f/2 + f_e]T'} \right.$$

$$\left. + \frac{i}{\pi\Delta f(\ell-m)} \left(e^{i2\pi[(\ell-m)\Delta f/2 + f_e]T'} - 1 \right) \right] \quad (15)$$

$$b' = b + a\,t' \quad (16)$$

Thus, the low frequency part of the filter output is reduced to a simple expression. The H and G functions need be evaluated only every Δt which may be much larger than T. It will become clear later that the phase of $R_{m\ell}\big|_{LF}$ is not important. Thus the phase factor in equation (14) need not be evaluated. If the filters are identical, the G and H functions become only functions of $m-\ell$, which then requires only 15 separate H and G coefficients rather than 64.

The high frequency contribution to the filter output is

$$R_{m\ell}\Big|_{HF} = \frac{E_o}{N} \int_0^{T'} \frac{1}{2L} \sum_{n=n_c+1}^{\infty} \left(C_n e^{\frac{in\pi t}{L}} + C_{-n} e^{\frac{-in\pi t}{L}}\right) e^{i2\pi[(\ell-m)\Delta f/2 + f_e]t} dt \quad (17)$$

These frequencies, since they are faster than a chip period are assumed to contribute as random gaussian noise in the filters. After integrating and averaging, the variance of the filter output is

$$\overline{R_{m\ell}^* R_{m\ell}}\Big|_{HF} = \frac{E_o^2 T'^2}{2N^2 L} \sum_{n=n_c+1}^{\infty} \frac{\overline{C_n^* C_n}}{2L} \left\{ Sinc\left[((\ell-m)\Delta f/2 + n/2L + f_e)T'\right] \right.$$

$$\left. + Sinc\left[((\ell-m)\Delta f/2 - n/2L + f_e)T'\right] \right\} \quad (18)$$

$$\equiv 2F_{m\ell}(T', f_e) \quad (19)$$

where $\dfrac{\overline{C_n^* C_n}}{2L}$ is the signal power spectral density and $Sinc(x) = \sin^2(x)/x^2$. This treatment of the higher frequency components assumes that $\overline{R_{m\ell} R_{m\ell}}$ equals zero and that the filter outputs from these components for each successive chip are independent. The first assumption is always true since propagation studies demonstrate that the signal structure is Rayleigh before significant power is found at these higher frequencies. The second assumption is an approximate result of specifying $n_c = L/T$.

The final filter contribution is due to noise, which is assumed to be gaussian, white, and equal in all filters. It is easy to demonstrate that the noise output has a variance of

$$2d^2 = 2E_o^2 T/N \quad (20)$$

which is four times the chip energy to noise ratio. The term can, for convenience, be added to $\overline{R_{m\ell}^* R_{m\ell}}$ since both are variances of independent gaussian variables.

The output of the mth filter where the signal was transmitted in the ℓth is

24

$$R_{m\ell} = a\, H_{m\ell}(T',f_e) + (b + at')\, G_{m\ell}(T',f_e) + (F_{m\ell}(T',f_e) + d^2)^{1/2}(G(o) + i\, G(o))$$

$$(21)$$

where $G(o)$ is a gaussian sample of unit variance. This particular model allows for the effects of timing errors, frequency errors, and scintillation induced phase and amplitude effects without being complex or expensive to execute.

The matched filter outputs are each envelope detected, which corresponds to taking the absolute value of $R_{m\ell}$. The resulting scalar quantities are quantized to integer quantities with a maximum of 15 and then processed for acquisition or information decoding.

The next piece of hardware to be considered is the automatic gain control (AGC). The AGC maintains the signal power into the demodulator filters so that the average envelope detection output after quantization is 5.5 with only noise present. As S/N becomes very large, assuming $f_e = T_e = 0$, the output of the envelope detector following the filter containing the signal approaches 25. Note that the quantization truncates this value to 15. It is necessary to model the AGC because some of the information processing is dependent on thresholds for the quantized outputs. The dynamic response of the AGC is modeled as exponential. For a step function increase in signal strength, the gain signal decreases exponentially to its new level with a time constant of 16 milliseconds. For a step decrease, the time constant is 80 milliseconds. This asymmetry in response degrades the system when the signal fluctuations become comparable to these response times since the signal level is depressed by the asymmetry. This question was not examined in detail since, as will be shown later, the severest system degradation occurs for circumstances where AGC effects are not significant.

The modeling of the system processes is straightforward given the hardware models already described. First, using Fourier techniques found in the appendix, sample signal structures are generated. This signal is then used to calculate the relevant AGC—filter—envelope—detector— quantizer outputs for each successive chip. These outputs are processed according to the description of the acquisition and decoding procedures discussed in the last section. The results are finally accumulated in terms of various statistical measures shown in section V.

25

SECTION V

SIMULATION RESULTS

Figure 8 contains the results of the acquisition study. The results are characterized by four regions. The first $(0.7\ r_0/\ \bar{v} \leq \tau_0 \leq 1.4\ r_0/\ \bar{v})$ is a transition region from no degradation effects to relatively constant effects. The transition region is relatively small and is located at $\tau_0 = r_0/\ \bar{v}$. The signal statistics in this region are generally nonRician and not amenable to simple descriptions as are the other regions.

The second region $(0.2 \leq \tau_0 \leq 0.7 r_0/\ \bar{v})$ of relatively constant system performance is the most important region as it represents the worst system performance over most of the likely range of τ_0. The relatively constant performance is a result of the fact that the signal fluctuations are slow compared to the effective integration periods of the acquisition algorithms.

The third region $(0.03 \leq \tau_0 \leq 0.2)$ shows a recovery of the acquisition performance caused by the integration properties of the acquisition algorithms as τ_0 becomes smaller. Finally, the fourth region $(\tau_0 \leq 0.02)$ shows a system degradation caused by an increase in scintillation induced cross-talk. The cross-talk becomes important when $1/\tau_0$ approaches the frequency separation of the matched filters.

This study indicates that about 18 dB of S/N are required to get a 0.84 or greater probability of acquisition for any ambient environment at 18 dB or above. Most of the failures in acquisition were due to failure in recognizing the start of message characters. The initial hopping pattern recognition and the time and frequency pull-in, in general, worked well even with a severely scintillated signal.

Figure 9 shows the ambient acquisition performance along with the performance in the $\tau_0 = 1.9$ second environment. The second curve represents a limiting case of the acquisition performance for any nonnuclear environment.

After successful acquisition, the system must be able to decode the information in the signal. Three aspects of this problem were examined. First, the ability to maintain time and frequency tracking was considered. None of the environments considered here seriously affected the time and frequency
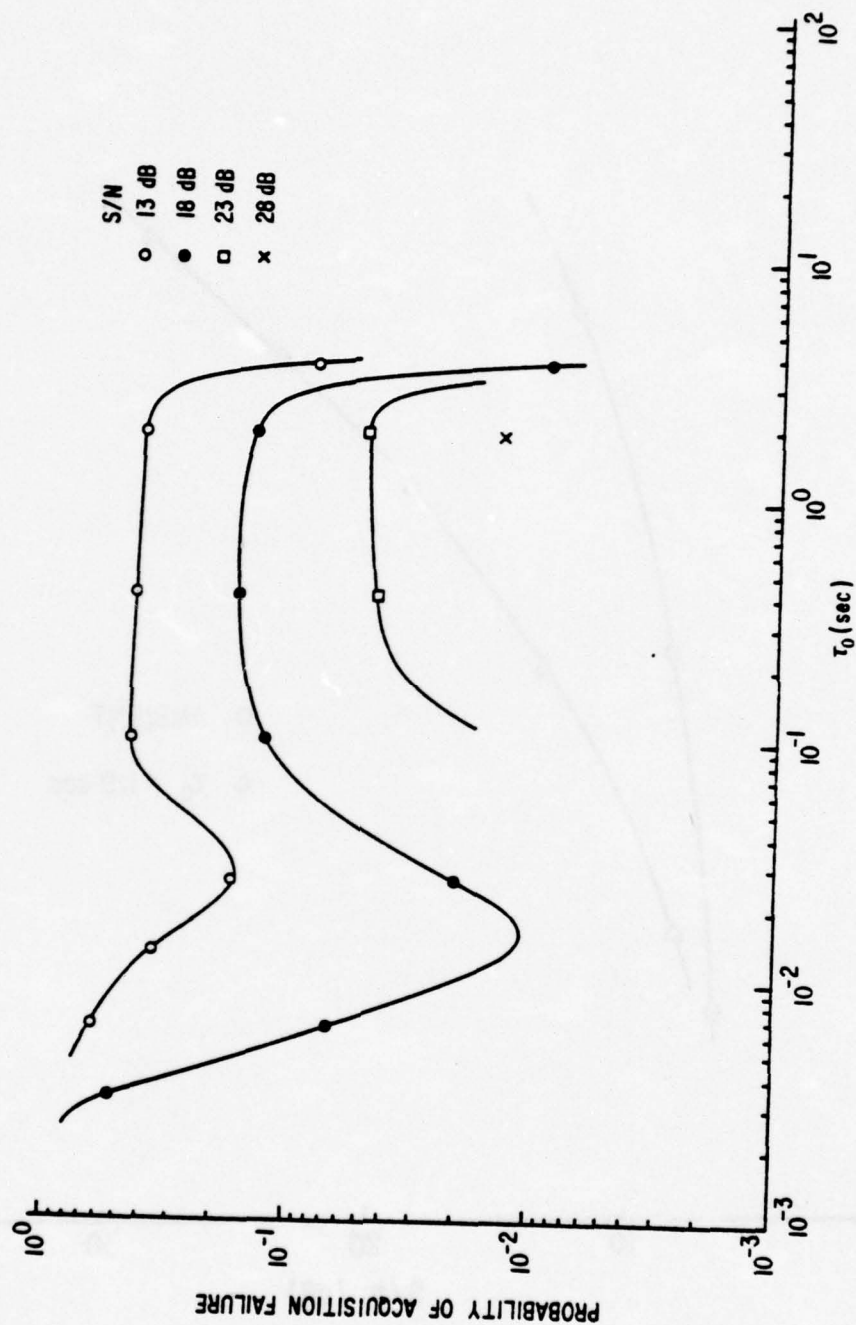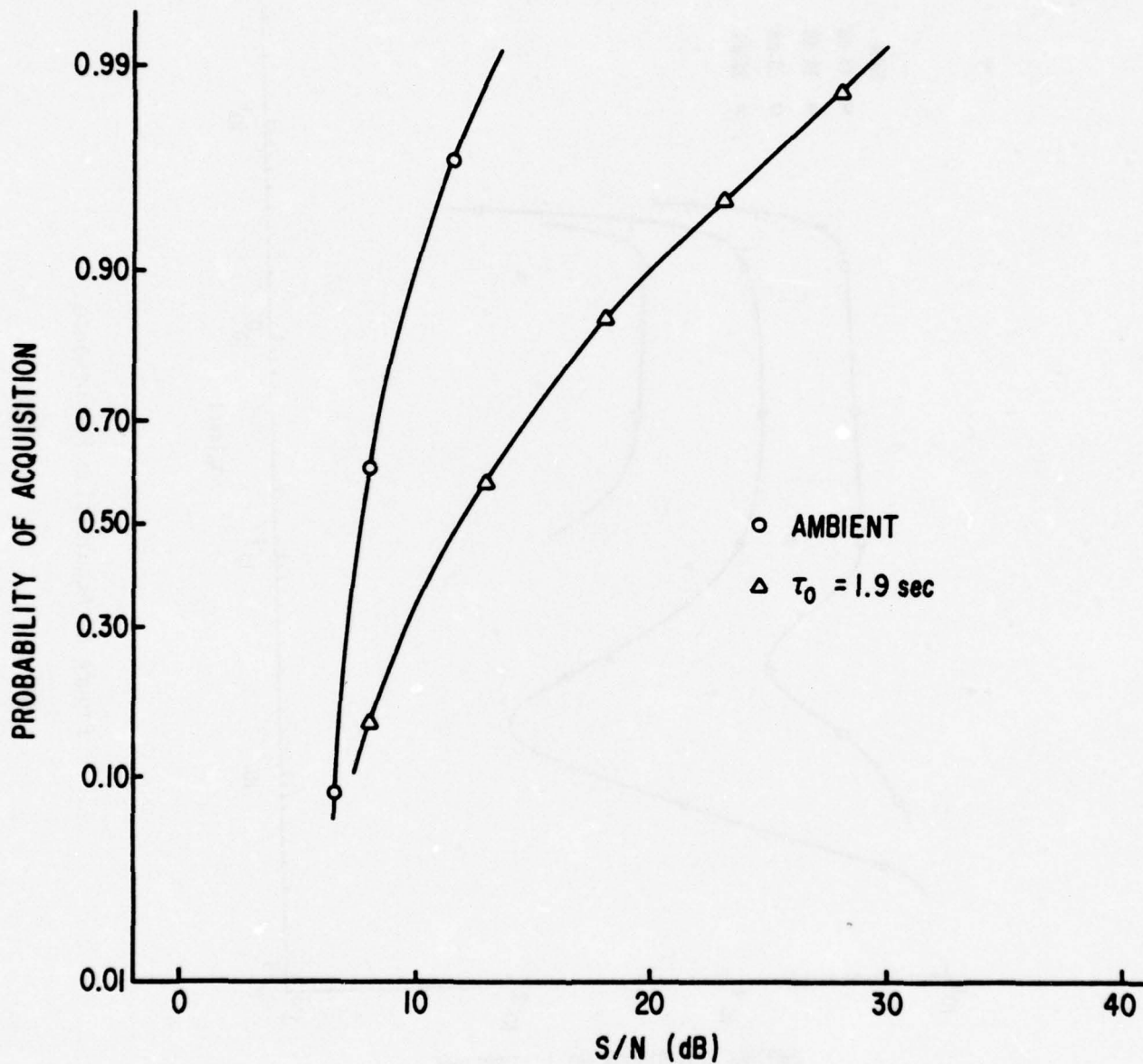
Figure 8. Acquisition Performance

Figure 9. Ambient and Disturbed Acquisition Performance

tracking behavior. Second, the decoder must correctly recognize the characters sent. Figure 10 shows the 6 bit character error rate as a function of τ_0 and S/N. The performance curves are similar in character to the acquisition curves for the same basic reasons. Figure 11 has the ambient performance along with the results of the τ_0 = 0.013 and 1.93 second environments. The τ_0 = 1.93 curve can be considered as a limiting performance curve for any ambient environment. In using the curves in figures 10 and 11, it must be remembered that the character errors are not random in time. Figures 12 and 13 show the simulation results for a string of characters at S/N of 18 dB and 13 dB with τ_0 = 1.9 seconds where the dashes represent incorrectly received characters. The nonrandom nature of the errors is clearly evident. The effects of the nonrandomness of the errors depends on the nature of the message itself; but, in general, nonrandom errors are not desirable.

Earlier, in section II, it was shown that propagation effects can be extrapolated from a single propagation calculation if that calculation is reasonably near the gaussian limit of the correlation functions of the quadrature components. Figure 10 shows, for S/N = 18 dB, the system performances for a few cases extrapolated from the τ_0 = 0.4 case. The extrapolated results agree well with the nonextrapolated calculations. The extrapolated result at τ_0 = 4 is what would have happened if $\bar{v}$ were a bit smaller or r_0 a bit larger causing the onset of effects to occur at larger τ_0.

The numerical error in figure 10 and those following is primarily due to jitter from the Monte Carlo aspect of the calculation. For $\tau_0 \geq 0.05$, the estimated error is less than 20 percent relative; and for $\tau_0 < 0.05$, the estimated error is less than 50 percent relative. A factor of about 2 was added to these error estimates over the actual estimated numerical error to account for the uncertainties in the numerical modeling. Unfortunately, available system performance information was insufficient to evaluate the accuracy of the numerical models even with nonperturbed signals.

The third aspect of the decoding examined was the loss of message algorithm. Figure 14 shows the average turn-off time for S/N = 18 dB. For $0.2 \leq \tau_0 \leq 0.7$ $r_0/\bar{v}$, the system would disable itself after only 10 seconds on the average. This is clearly not acceptable, but fortunately the loss of message threshold, CTR, is adjustable. Figure 15 shows the average turn-off time as a function of CTR with S/N = 18 dB and τ = 0.4. The problem can be corrected by lowering CTR but at the cost of not recognizing the loss of signal as readily. Since
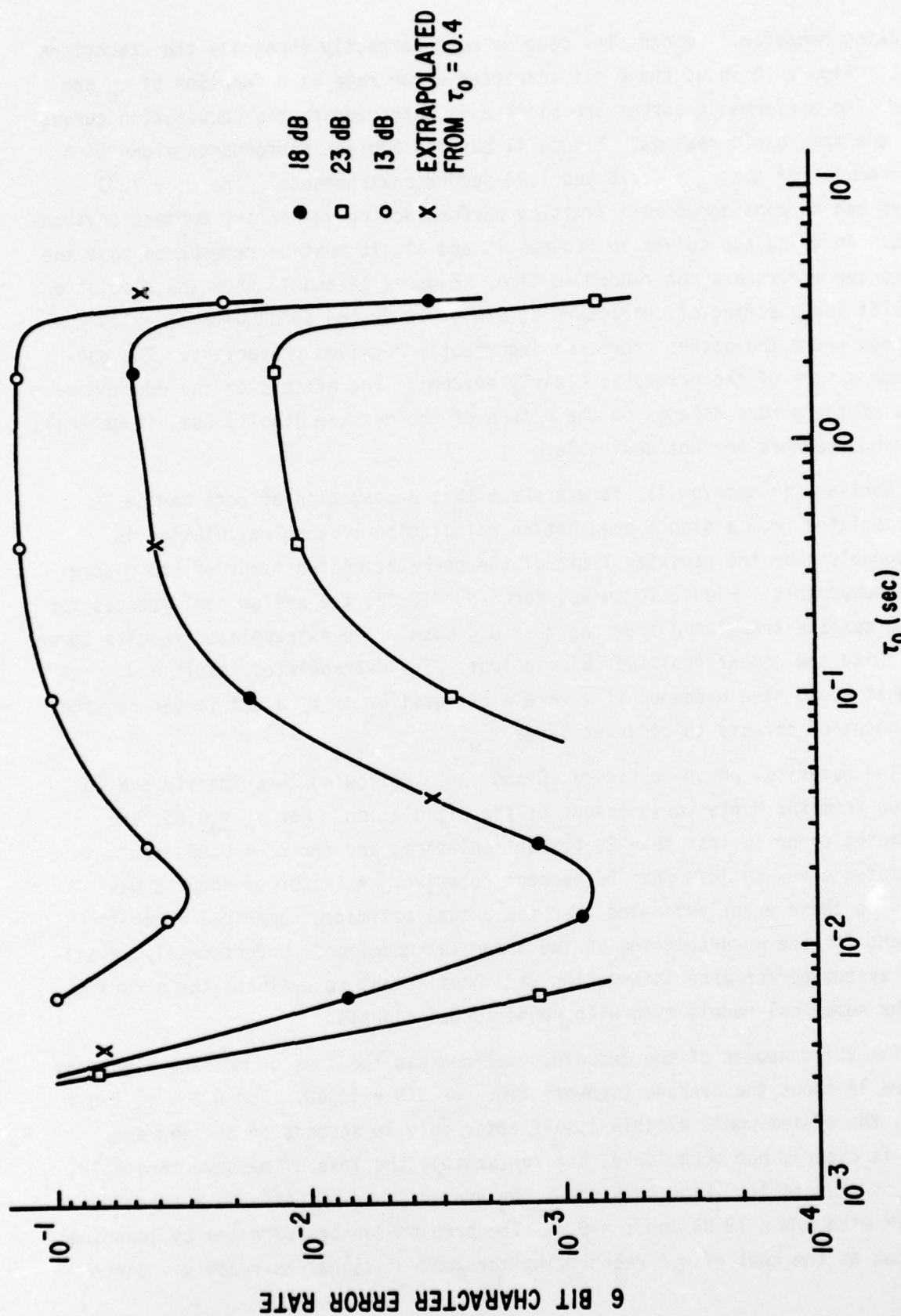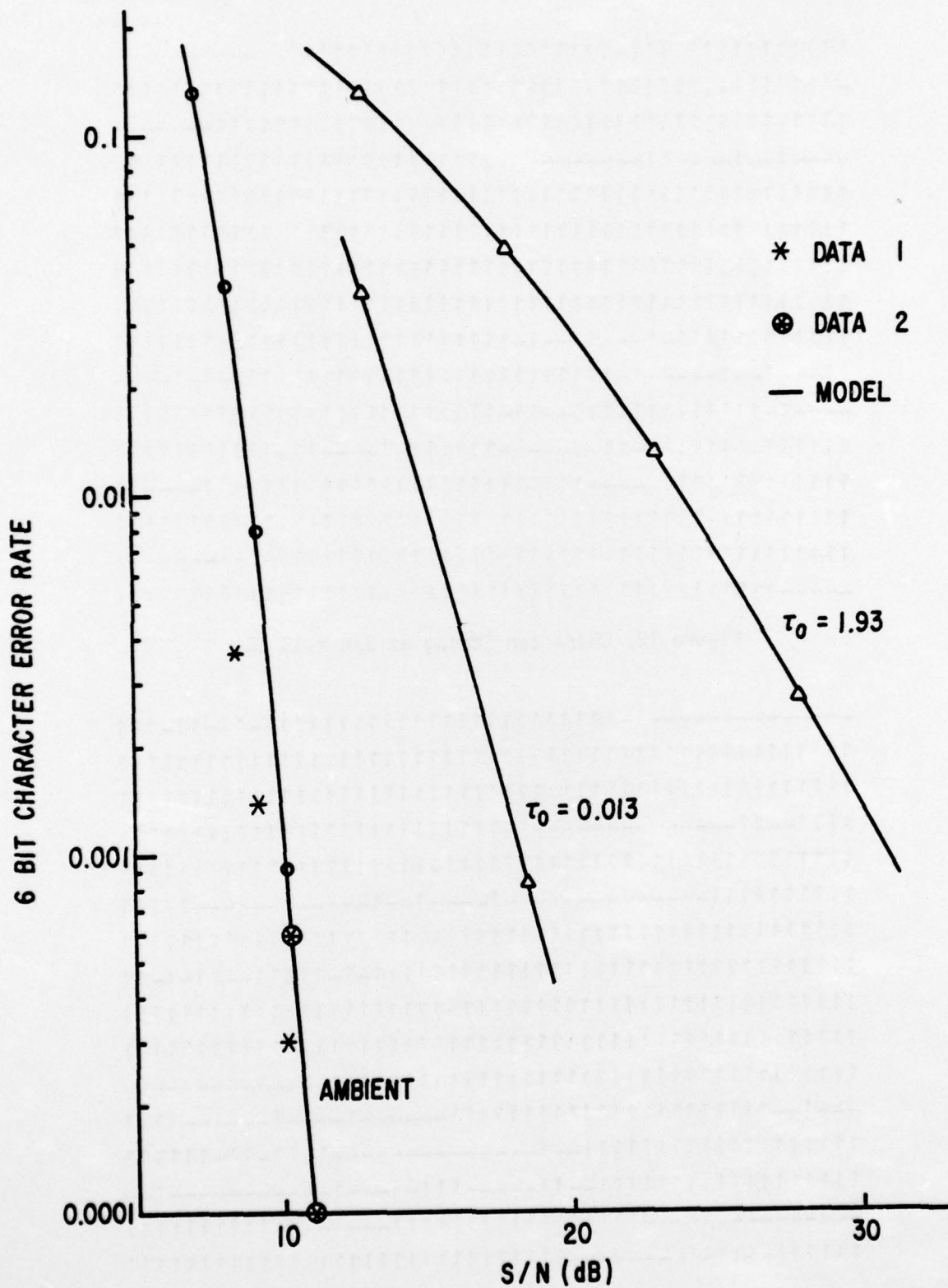
Figure 10. Character Decoding Performance

Figure 11. 6 Bit Character Error Rate

```
11111111111111111111111111111111111111---------- ------- -----
-1111111111111111111111111111111111111111111111111111111
11111111111111111111111111111111111111  11111111----------
----1--1-----11----------1111111111111111111111111  11
11111111111111111111111111111111111111111111111111111111111
11111111111111111111111111111111111111111111111111111111111
11111111111111111111111111111111111111111111111111111111111
1111111111111111111111111111111111111111111111111111111111
111111111111111-1---1---1-11111111111111111111111111111111
-1-1-1--1--1------1-111111111111111111111111111-1-1------
----1-1111111111111---11-1111111111111111111111111111111
1111111111111111---11-1------111111-1-----11-11111111111
1111111111111111-----1111111111111111111111111----11
1111111111111111111111111111111111111111111111111111111111
11111111111111111111111111111111111111111111111-1----------
------11111111111111111111111111111111111111111111111
```

Figure 12. Character String at S/N = 18 dB

```
----------------1-11111111111111111111111111-1--11-111
1111111111111111111111111111111111111111111111111111111
11111111111111111111111111111111111111111111111111111111
1111---11----------------1-1111111111111111111111111111
11111111111111111111111111111111111111111111111111111111
1111111111----------------1----1--1----------------11111
11111111111111111111111111111111111111111111111111111111
11111111111111111111111111111111-1-11111-111-1-11
1111111111111111111111111111111111111111111111111111111
11111111111111111111111111111111111111111111111111111111
11111111111111111111111111111111111111---1----------
---1--111111111111111111111111-------1----1---1--11-1
11111111111111111111--1---------------1-11-11-111111
11111111111111111111--11-----111-1---1-----------1--
----------------1111111111111111111-------1-1111111111
1111111111-1--------1111111111111111111111111111111111
```

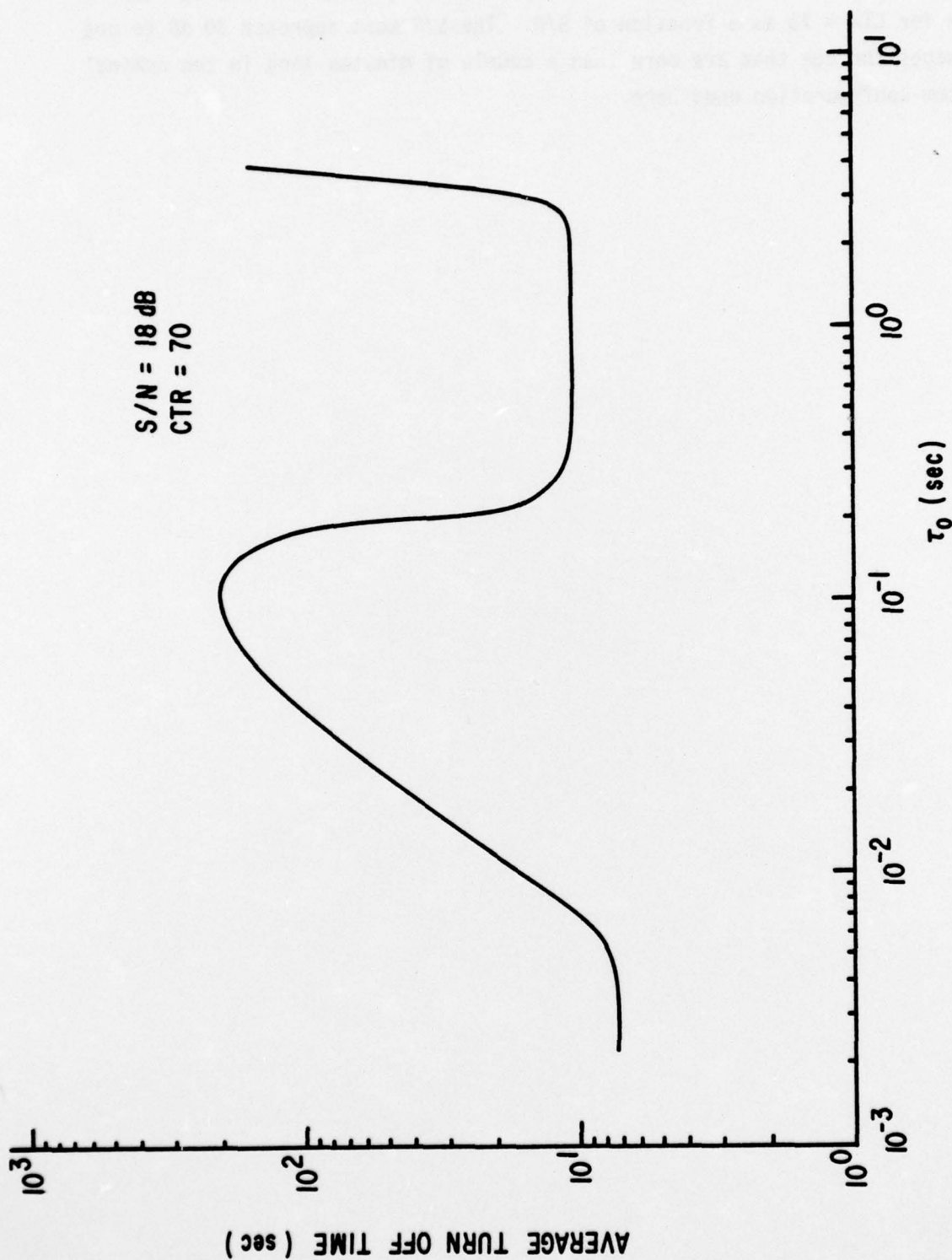Figure 13. Character String at S/N = 13 dB

32

Figure 14. Loss of Message Performance

the lower limit of CTR is 48, it seems clear that 18 dB of S/N is required for reasonable system performance. Finally, figure 16 shows the average turn-off time for CTR = 70 as a function of S/N. The S/N must approach 30 dB to get messages through that are more than a couple of minutes long in the nominal system configuration used here.
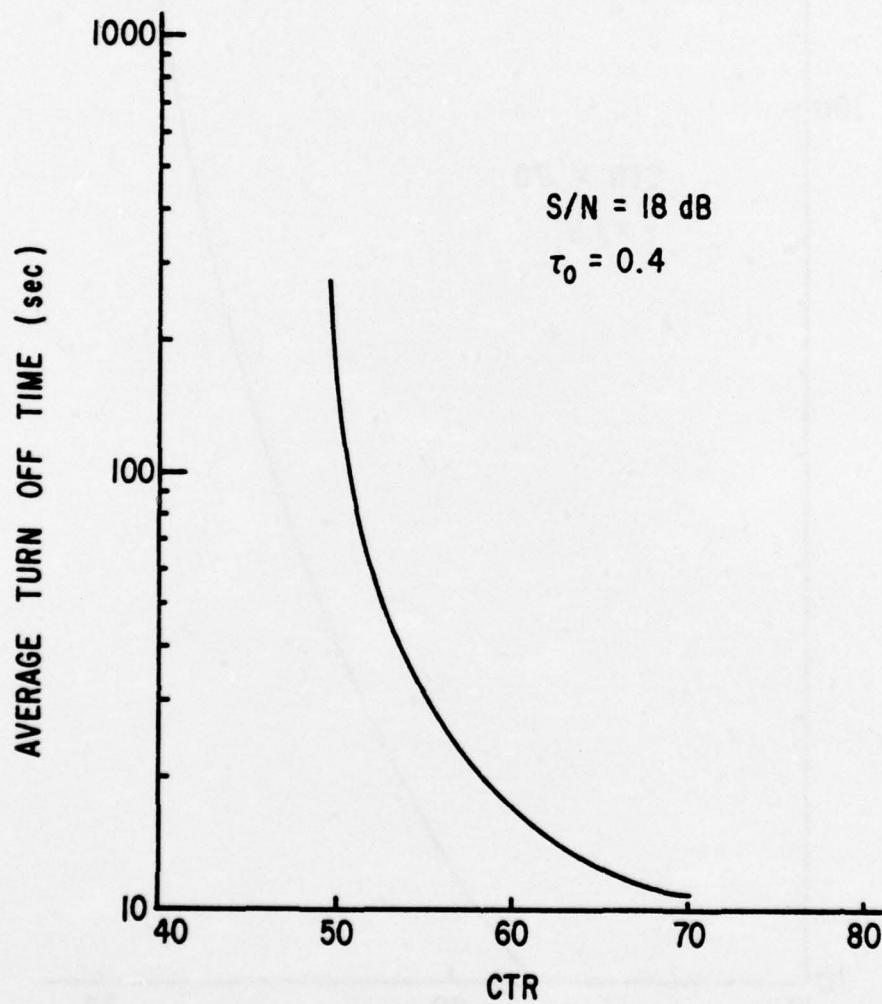
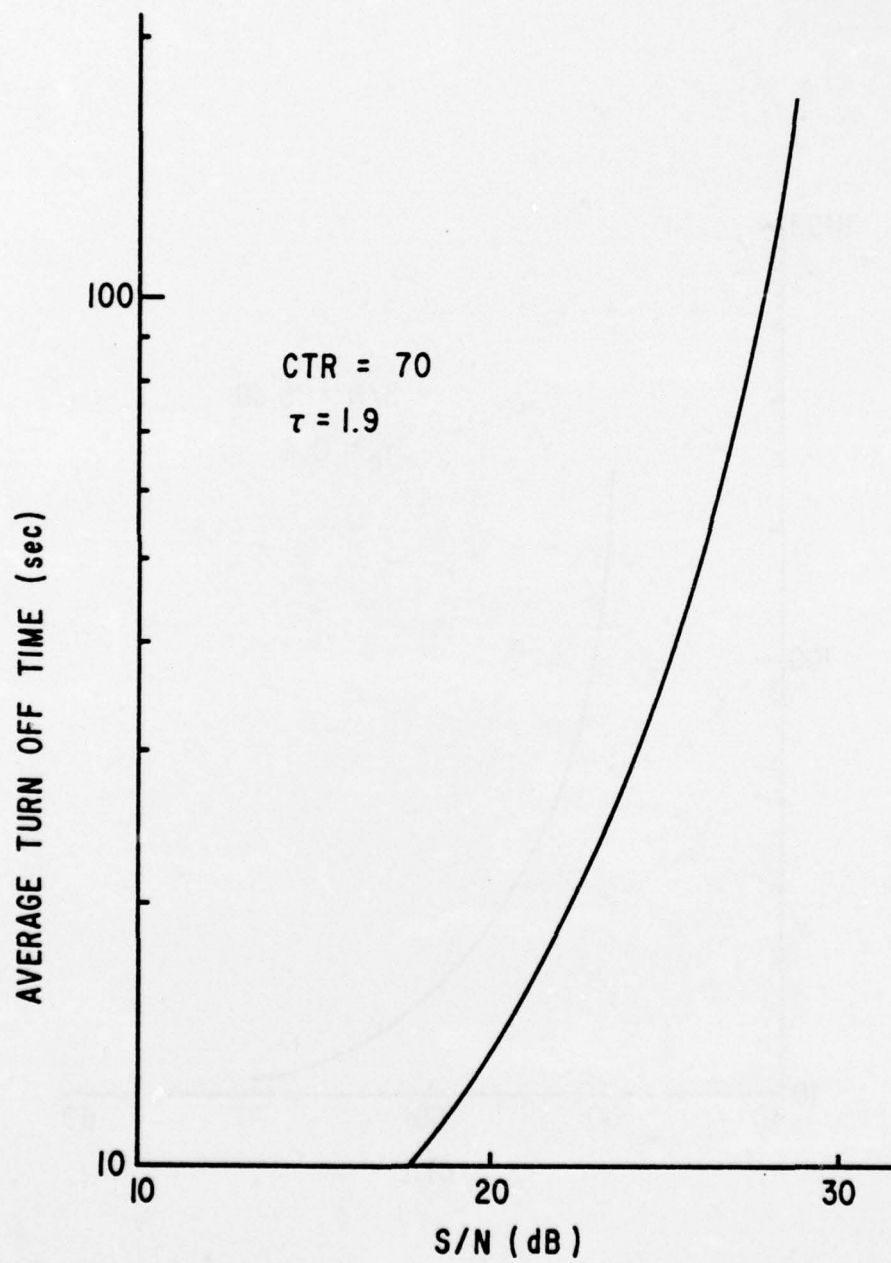Figure 15. Loss of Message Performance as a Function of CTR

Figure 16. Average Turn Off Time Versus S/N

SECTION VI

CONCLUSIONS AND RECOMMENDATIONS

1. The loss of message algorithm posed the most serious problem. For the nominal configuration assumed for this study, an S/N of about 28 dB is required to get message lengths of 2 minutes or longer. This problem can be alleviated by lowering the loss of message threshold. With the minimum setting of the threshold, messages of several minutes duration will be received at 18 dB. It is recommended that this problem be examined further, preferably by testing the real hardware.

2. Neglecting the loss of message problem, the system worked marginally well at 18 dB. The probability of acquisition was 0.84 and the 6 bit character rate was about 0.05. Operation at this level requires toleration of character error behavior as shown in figure 12. Figures 9 and 11 contain worst case system performance curves for any perturbed nonnuclear environment.

3. The ultimate limit in system performance as the environment becomes more severe is set by the chip period and the filter separation. If either $\tau_0 \ll T$ or $\tau_0 \ll 1/\Delta f$, then the system performance is irrecoverable for practical S/N.

4. The use of the Reed-Solomon code resulted in a significant improvement in system performance due to the orthogonality of the character representations and the integration effect of the code over the character length.

5. UHF propagation is sufficiently well understood that worst case performance curves can be developed for UHF systems. This means that system specifications and the means to test for compliance are now practical for scintillation effects.

6. It is recommended that a signal processor be developed to simulate scintillation effects for system test purposes. Because of the complexity of these systems, it is not likely that sufficient confidence in survivability can be gained from simulations such as done here.

REFERENCES

1. Phelps, A.D.R., and Sagalyn, R.C., "Plasma Density Irregularities in the High-Latitude Top Side Ionosphere," Journal of Geophysical Research, Vol. 81, No. 4, 1 February 1976.

2. Dyson, P.L., McClure, J.P., and Hanson, W.B., "In Situ Measurements of the Spectral Characteristics of F Region Ionospheric Irregularities," Journal of Geophysical Research, Vol. 79, 1 April 1974.

3. Wittwer, L.A., Satellite Communications in a Scintillated Environment, AFWL-TR-75-240, January 1976.

4. Rhino, C.L., "Some Unique Features of the Transionospheric Channel," to appear in the Proceedings of the 1975 Symposium on the Effect of the Ionosphere on Space Systems and Communications, 20-22 January 1975.

5. Bogusch, R.L., "Ionospheric Scintillation Effects on Satellite Communications: Interim Technical Note," Mission Research Corporation, MRC-N-139, June 1974.

6. Air Force Satellite Communication System-Training Manual-Systems Overview, 523-0765641-002118, Collins Radio Group, Rockwell International, 28 February 1975.

7. Paulson, M.R., and Hopkins, R.V.F., Effects of Equatorial Scintillation Fading on SATCOM Signals, Naval Electronics Laboratory Center TR 1875, 8 May 1973.

APPENDIX

GENERATION OF COMPLEX CORRELATED RANDOM SEQUENCES

Let $f(t)$ be a zero mean random gaussian variable on the domain $(-T,T)$. $f(t)$ can be expanded in a Fourier series.

$$f(t) = \frac{1}{2} \sum_{n=-\infty}^{\infty} C_n \ell^{i\omega_n t}, \quad \omega_n = \frac{n\pi}{T} \tag{A1}$$

$$C_n = \frac{1}{T} \int_{-T}^{T} f(t) \, \ell^{-i\omega_n t} \, dt \tag{A2}$$

Let

$$G(t-t') = \overline{f^*(t)f(t')} \tag{A3}$$

$$F(t-t') = \overline{f(t)f(t')} \tag{A4}$$

Then

$$\underset{T\to\infty}{\text{Lim}}(\overline{TC_n^* \, C_m}) = 0, \quad m \neq n, \, m \neq 0 \tag{A5}$$

$$\underset{T\to\infty}{\text{Lim}}(\overline{TC_m^* \, C_m}) = 4 \int_0^{2T} d\alpha \, G(\alpha) \cos(\alpha\omega_m) \tag{A6}$$

$$= T \, K_m$$

$$\underset{T\to\infty}{\text{Lim}}(\overline{TC_n \, C_m}) = 0, \quad m \neq n, \, m \neq 0 \tag{A7}$$

$$\underset{T\to\infty}{\text{Lim}}(\overline{TC_m \, C_{-m}}) = 4 \int_0^{2T} d\alpha \, F(\alpha) \cos(\alpha\omega_m) \tag{A8}$$

$$= T(L_m + i \, M_m)$$

If T is chosen such that $F(t) = G(t) \approx 0$ for $t \geq T$, the limits in equations (A5), (A6), (A7), and (A8) can be assumed. Now if $C_m = C_{mr} + iC_{mi}$, and using equations (A5), (A6), (A7), and (A8), then with $m \neq 0$,

$$\overline{C_{mr} \, C_{mr}} = \overline{C_{mi} \, C_{mi}} = K_m/2 \tag{A9}$$

$$\overline{C_{mr} \, C_{mi}} = 0 \tag{A10}$$

$$\overline{C_{mr} \, C_{-mr}} = \overline{-C_{mi} \, C_{-mi}} = L_m/2 \tag{A11}$$

$$\overline{C_{mr} \, C_{-mi}} = \overline{C_{-mr} \, C_{mi}} = M_m/2 \tag{A12}$$

Since C_{mr}, C_{mi}, C_{-mr}, and C_{-mi} are random gaussian variables, the joint probability distribution function of these variables can be written in terms of K_m, L_m, and M_m.

$$P(C_{mr}, C_{mi}, C_{-mr}, C_{-mi}) = C \exp$$

$$\left\{ \frac{\begin{bmatrix} |C_{mr} \ C_{mi} \ C_{-mr} \ C_{-mi}| \end{bmatrix} \begin{bmatrix} K_m & 0 & -L_m & -M_m \\ 0 & K_m & -M_m & L_m \\ -L_m & -M_m & K_m & 0 \\ -M_m & L_m & 0 & K_m \end{bmatrix} \begin{bmatrix} C_{mr} \\ C_{mi} \\ C_{-mr} \\ C_{-mi} \end{bmatrix}}{(K_m{}^2 - L_m{}^2 - M_m{}^2)} \right\} \tag{A13}$$

This expression can be simplified by diagonalizing the 4 x 4 matrix. To diagonalize the above matrix, a transformation matrix must be found with the following properties.

$$T^{-1}T = TT^{-1} = I \tag{A14}$$

$$T \, Q \, T^{-1} = R \tag{A15}$$

where I is the identity matrix, Q is the 4 x 4 matrix in equation 13, and R is a diagonal matrix with diagonal elements λ_1, λ_2, λ_3, and λ_4. The diagonal elements are easily solved for

$$\lambda_1 = \lambda_2 = K_m + \sqrt{L_m^2 + M_m^2} \tag{A16}$$

$$\lambda_3 = \lambda_4 = K_m - \sqrt{L_m^2 + M_m^2} \tag{A17}$$

A matrix, T, with the desired properties is

$$T = \frac{1}{\sqrt{2}} \begin{vmatrix} 1 & 0 & L_m/\sqrt{} & M_m/\sqrt{} \\ 0 & 1 & M_m/\sqrt{} & -L_m\sqrt{} \\ -L_m/\sqrt{} & -M_m/\sqrt{} & 1 & 0 \\ -M_m\sqrt{} & L_m/\sqrt{} & 0 & 1 \end{vmatrix} \tag{A18}$$

where $\sqrt{} = \sqrt{L_m^2 + M_m^2}$. The probability density function can now be written as

$$P(C_{mr}', C_{mi}', C_{-mr}', C_{-mi}') = C' \exp$$

$$\left\{ -\frac{1}{2} \left[\frac{2(C_{mr}'^2 + C_{mi}'^2)}{K_m + \sqrt{L_m^2 + M_m^2}} + \frac{2(C_{-mr}'^2 + C_{-mi}'^2)}{K_m - \sqrt{L_m^2 + M_m^2}} \right] \right\} \tag{A19}$$

where

$$\begin{vmatrix} C_{mr} \\ C_{mi} \\ C_{-mr} \\ C_{-mi} \end{vmatrix} = \frac{1}{\sqrt{2}} \begin{vmatrix} 1 & 0 & -L_m/\sqrt{} & -M_m/\sqrt{} \\ 0 & 1 & -M_m/\sqrt{} & L_m/\sqrt{} \\ L_m/\sqrt{} & M_m/ & 1 & 0 \\ M_m/\sqrt{} & -L_m/ & 0 & 1 \end{vmatrix} \begin{vmatrix} C_{mr}' \\ C_{mi}' \\ C_{-mr}' \\ C_{-mi}' \end{vmatrix} \tag{A20}$$

The primed variables are also random gaussian variables with variances as shown in equation (A19). Generating a simple of f(t) on the interval $-T \leq t \leq T$ is now straightforward. For each $m \neq 0$, sample a gaussian distribution four times

41

to get values of C'_{mr}, C'_{mi}, C'_{-mr}, and C'_{-mi}, transform using equation (20) to unprimed variables, and form the random Fourier coefficient by $C_m = C_{mr} + iC_{mi}$. For $m = 0$, another procedure must be used. From equations (A6) and (A8)

$$\overline{C_{or}^2} + \overline{C_{oi}^2} = K_o \tag{A21}$$

$$\overline{C_{or}^2} - \overline{C_{oi}^2} = L_o \tag{A22}$$

$$\overline{C_{or}\,C_{oi}} = M_o/2 \tag{A23}$$

Thus

$$\overline{C_{or}^2} = (K_o + L_o)/2 \tag{A24}$$

$$\overline{C_{oi}^2} = (K_o - L_o)/2 \tag{A25}$$

The joint probability function can now be written as

$$P(C_{or}, C_{oi}) = C \exp\left\{\left[\frac{|C_{oi}\ C_{or}|\begin{vmatrix} (K_o-L_o) & -M_o \\ -M_o & (K_o+L_o) \end{vmatrix}\begin{vmatrix} C_{oi} \\ C_{or} \end{vmatrix}}{(K_o^2-L_o^2-M_o^2)}\right]\right\} \tag{A-26}$$

Following the same procedure as with $m \neq 0$, the probability matrix can be diagonalized.

Let

$$C_{or} = [(K_o+L_o)/2]^{1/2}\left(C'_{or} + C'_{oi}\right) \tag{A-27}$$

$$C_{oi} = [(K_o-L_o)/2]^{1/2}\left(C'_{or} - C'_{oi}\right) \tag{A-28}$$

42

Then

$$P(C'_{or}, C'_{oi}) = C \exp\left\{ -\frac{1}{2}\left[\frac{2(K_o^2 - L_o^2 - M_o (K_o^2 - L_o^2)^{1/2}}{K_o^2 - L_o^2 - M_o^2} C'^2_{or} \right.\right.$$

$$\left.\left. + \frac{2(K_o^2 - L_o^2 + M_o \left(K_o^2 - L_o^2\right)^{1/2})}{K_o^2 - L_o^2 - M_o^2} C'^2_{oi} \right]\right\}$$

$$= C \exp\left\{ -\frac{1}{2}\left[\frac{C'^2_{or}}{\sigma_r^2} + \frac{C'^2_{oi}}{\sigma_i^2} \right]\right\} \tag{A30}$$

To generate C_{or} and C_{oi}, a random gaussian sample of C'_{or} and C'_{oi} are generated with the variances $\sigma_r{}^2$ and $\sigma_i{}^2$, respectively, and used in equations (A27) and (A28). After the random complex Fourier coefficients are found for all m, the sample f(t) is calculated by inverse Fourier transforming as in equation (A1).